ORIGINAL ARTICLE

Mapping of breakpoints in balanced chromosomal translocations by shallow whole-genome sequencing points to *EFNA5*, *BAHD1* and *PPP2R5E* as novel candidates for genes causing human Mendelian disorders

Victor Murcia Pienkowski,[1,2] Marzena Kucharczyk,[3] Marlena Młynek,[3] Krzysztof Szczałuba,[1] Małgorzata Rydzanicz,[1] Barbara Poszewiecka,[4] Agata Skórka,[3,5] Maciej Sykulski,[1,6] Anna Biernacka,[1,2] Agnieszka Anna Koppolu,[1,2] Renata Posmyk,[7,8] Anna Walczak,[1] Joanna Kosińska,[1] Paweł Krajewski,[9] Jennifer Castaneda,[10] Ewa Obersztyn,[10] Elżbieta Jurkiewicz,[11] Robert Śmigiel,[12] Anna Gambin,[4] Krystyna Chrzanowska,[3] Małgorzata Krajewska-Walasek,[3] Rafał Płoski[1]

► Additional material is published online only. To view please visit the journal online (http://dx.doi.org/10.1136/jmedgenet-2018-105527).

For numbered affiliations see end of article.

Correspondence to
Professor Rafał Płoski, Department of Medical Genetics, Medical University of Warsaw, Warsaw 02-106, Poland; rploski@wp.pl

VMP, MK and MM contributed equally.

Received 10 June 2018
Revised 21 September 2018
Accepted 22 September 2018
Published Online First 23 October 2018

To cite: Murcia Pienkowski V, Kucharczyk M, Młynek M, *et al*. *J Med Genet* 2019;**56**:104–112.

ABSTRACT

Background Mapping the breakpoints in de novo balanced chromosomal translocations (BCT) in symptomatic individuals provides a unique opportunity to identify in an unbiased way the likely causative genetic defect and thus find novel human disease candidate genes. Our aim was to fine-map breakpoints of de novo BCTs in a case series of nine patients.

Methods Shallow whole-genome mate pair sequencing (SGMPS) together with long-range PCR and Sanger sequencing. In one case (BCT disrupting *BAHD1* and *RET*) cDNA analysis was used to verify expression of a fusion transcript in cultured fibroblasts.

Results In all nine probands 11 disrupted genes were found, that is, *EFNA5*, *EBF3*, *LARGE*, *PPP2R5E*, *TXNDC5*, *ZNF423*, *NIPBL*, *BAHD1*, *RET*, *TRPS1* and *SLC4A10*. Five subjects had translocations that disrupted genes with so far unknown (*EFNA5*, *BAHD1*, *PPP2R5E*, *TXNDC5*) or poorly delineated impact on the phenotype (*SLC4A10*, two previous reports of BCT disrupting the gene). The four genes with no previous disease associations (*EFNA5*, *BAHD1*, *PPP2R5E*, *TXNDC5*), when compared with all human genes by a bootstrap test, had significantly higher pLI ($p<0.017$) and DOMINO ($p<0.02$) scores indicating enrichment in genes likely to be intolerant to single copy damage. Inspection of individual pLI and DOMINO scores, and local topologically associating domain structure suggested that *EFNA5*, *BAHD1* and *PPP2R5E* were particularly good candidates for novel disease loci. The pathomechanism for *BAHD1* may involve deregulation of expression due to fusion with *RET* promoter.

Conclusion SGMPS in symptomatic carriers of BCTs is a powerful approach to delineate novel human gene–disease associations.

INTRODUCTION

Balanced chromosomal translocations (BCT) cause exchange of genetic material between non-homologous chromosomes without any change in the amount of DNA.[1] De novo BCTs have a frequency of 1 per 2000 live births.[2] Most individuals with BCTs are healthy, nonetheless in up to 26.8% of cases, BCTs are associated with clinical pathology.[3] Symptomatic BCTs provide a unique opportunity to identify the causative genetic mechanism as it is likely that such a mechanism is directly related to genome damage inflicted by the breakpoint(s).

BCT may cause a disease by direct disruption of a gene through intragenic break that is pathogenic through haploinsufficiency.[4] It is also possible that BCT creates a chimeric gene causing an expression of a novel protein or a novel promoter–gene combination. This mechanism occurring in somatic cells can cause cancer but there are also reports of similar germline events being responsible for mental retardation or psychiatric diseases.[5–8] Finally, the BCT breakpoint(s) may disrupt topologically associating domain (TAD) structure affecting regulatory elements and altering expression of genes that have not been directly damaged ,i.e. long-range position effect (LRPE).[9–11]

Historically, breakpoints in BCTs were mapped using karyotyping which was laborious and had limited resolution.[12 13] Next-generation sequencing (NGS) allowing whole-genome sequencing, in particular in the format of shallow genome mate pair sequencing (SGMPS), has considerably simplified identification of BCT breakpoints.[1 14]

In this study we present the results of de novo BCT mapping in a case series of nine symptomatic probands using SGMPS with a focus on cases where findings point to novel human disease candidate genes.

Patients

Written informed consent for all the genetic studies performed on the patients and their parents was obtained from the patients' legal guardians.

We studied nine symptomatic cases in whom de novo BCTs were found by standard karyotyping. The clinical inclusion criteria consisted of developmental delay, neurological dysfunction, congenital anomalies and/or dysmorphic features raising a suspicion of a known or novel genetically determined disease/syndrome. In all cases, translocations were confirmed as balanced by array comparative genomic hybridisation (aCGH). Furthermore, no de novo CNVs were found in any of the probands. The detailed clinical characteristic of five probands with breakpoint(s) in genes with unknown/poorly delineated disease phenotype is given below and summarised in table 1. Description of the remaining patients in whom the phenotype was considered as (likely/possibly) explained by the observed breakpoint(s) is shown in table 2.

Proband 1

The boy was the first child of healthy, non-consanguineous parents. The pregnancy was uneventful except for maternal hypothyroidism, treated effectively with thyroid hormone replacement. Birth weight at 39th week was 2160 g (<0.4th centile), length 48 cm (10th centile) and Apgar scores were 10 both at 1 and 5 min. At birth he was hypotonic, had bilateral cloudy cornea and several dysmorphic features. At 12 months he had square face; high forehead; bilateral epicanthic folds; sparse eyebrows; short and upturned nose; long and flat philtrum; narrow upper lip; micrognathia; small, dysplastic, posteriorly rotated and low-set ears; hypoplastic nipples; short distal phalanges of fingers; bilateral single palmar crease; syndactyly of second and third toes; and mild sandal gap.

Echocardiogram showed supravalvular pulmonary stenosis and atrial septal defect. Renal and cranial ultrasound was normal but abdominal ultrasound examination showed a portosystemic venous shunt. Consequent ultrasound and Doppler study of the abdomen revealed drainage of the left branch of the portal vein into the left hepatic vein and the boy was diagnosed with Abernethy malformation type II. The aberrant vessel was 3.3 mm in diameter. At 6 months the shunt was successfully occluded by embolisation with Amplatzer vascular plug.

The ophthalmologic evaluation revealed bilateral cloudy cornea caused by persistent corneal fetal vascularisation, but apparently without retinal involvement. Audiometric testing (auditory brainstem response (ABR), tympanometry and distortion product otoacoustic emissions (DPOAE)) performed at 2 months was normal.

Proband 2

The boy was born at 40th week with the following parameters: weight 3800 g (75th centile), length 59 cm (>90th centile), head circumference 35 cm (50th–75th centiles). The pregnancy was uncomplicated. Motor development was delayed: he sat unsupported at 6 months, walked unassisted at 18 months and said his first words at 2 years. At 21 years he was referred to genetic counselling unit due to moderate intellectual disability, hyperactivity features, coordination disorder and strange behavioural pattern consisting of sniffing. Body weight was 94 kg, height 194 cm (>97th centile) and occipitofrontal circumference (OFC) 57 cm (50th centile). He attends special school and has significant speech delay. His dysmorphism includes distal hand camptodactyly and unilateral transverse palmar crease. CT of the brain was normal.

Proband 3

The girl was born from the first pregnancy of healthy and non-consanguineous parents at 40th week with birth weight 2950 g (5th–10th centiles), length 52 cm (90th centile) and Apgar score of 7 (OFC was not measured). During the first week septic ileus developed and gastrostomy was performed followed by colectomy at 9 months due to Hirschsprung disease (Mendelian Inheritance in Man (MIM): 142623). Since 10 months of age the girl experienced recurrent urinary tract infections and, eventually, complement proteins deficit was diagnosed and appropriate treatment started. Her physical and psychomotor development was near normal up to 13 years when progressive intellectual deterioration occurred. Her IQ declined from 96 to 46 by 20 years. There were: learning difficulties, anxiety, depression, catatonic stupor, loss of previously gained abilities, incomprehensible speech and social withdrawal. A diagnosis of schizophrenia (paranoid type) was made. Electroencephalography (EEG) tracings showed generalised discharges of spikes as well as polyspike slow-wave pattern.

At 21 years her physical parameters were: weight 60 kg (75th centile), height 160 cm (25th centile) and OFC 55 cm (50th centile). She has large, soft and narrow hands with mild shortening of the metacarpals and long tapering fingers. Head MRIs at 11, 14 and 17 years showed irregular angiogenic lesions in the white matter of the paraventricular right frontoparietal region, the neighbourhood of the collateral trigone of the left lateral ventricle and frontal lobe. In addition, the lateral ventricles were slightly widened.

Proband 4

The girl was born to healthy parents at 40th week by caesarean section (fetal heart rate disturbances) with Apgar score of 10, weight 2830 g (5th–10th centiles), height 54 cm (90th centile) and head circumference 33 cm (5th centile). The pregnancy was complicated by oligohydramnios and maternal pre-eclampsia. In neonatal period, there was hypertonia which subsided after the 1 year of age. Motor development was slightly delayed: she sat unsupported at 8–9 months, walked unassisted at 15 months and said her first words at 1 year. Sleep disturbances were noted in infancy. The disproportion between body weight and height remained. At preschool age she experienced recurrent infections (bronchitis, pneumonia and strep throat), abdominal pains, aphthous stomatitis and bloating. She had unexplained bedwetting episodes. Ophthalmological examination revealed hyperopia and astigmatism, pigment dystrophy in the eye fundi and visual agnosia, and spatial apraxia.

At 12 years she was referred to a geneticist due to global developmental delay and low body weight of 35 kg (3rd centile) with height of 148 cm (3rd–10th centiles) and OFC 53 cm (25th centile). She attends a special school for children with impaired vision but have learning difficulties. Overall her cognitive development is good; vocabulary, knowledge and reasoning are adequate for age. Her dysmorphism includes subtle hirsutism, low back hairline, coarse facial features and rounded nasal tip. Brain MRI, EEG, urine amino and organic acids, plasma amino acids, and renal and abdominal ultrasound were normal. On aCGH, paternally inherited duplication at 3p22 was found. At 16 years the girl has mild intellectual delay and personality disorder, and suffers from self-mutilation.

Proband 5

The girl was born to healthy parents at 41st week from the first pregnancy with Apgar score of 9/10 in 1/5 min, weight 3620 g

Table 1 Characteristics of the probands with breakpoints in genes without known/well-established association with human diseases

	Proband 1	Proband 2	Proband 3	Proband 4	Proband 5
Current age	12 months	21 years	21 years	16 years	8 years
Karyotype	46,XY,t(5;8)(q22;q13)	46,XY,t(2;11)(q31;q21)	46,XX,t(10;15)(q11.2;q13)	46,XX,t(5,14)(q13.2;q24.3)	46,XX,t(6;14)(p25;q13)
Implicated genes	*EFNA5*	*SLC4A10*	*RET, BAHD1*	*PPP2R5E*	*BLOC1S5-TXNDC5, TXNDC5*
ExAC pLI*	0.889	0.003	0.991 (*BAHD1*)	0.999	0 (*TXNDC5*)
DOMINO score#	*0.992*	*0.205*	*0.634* (*BAHD1*)	*0.86*	*0.138* (*TXNDC5*)
Gene function	erythropoietin-producing human hepatocellular (EPH)-related receptor, tyrosine kinase ligand	Na(+) dependent Cl-/HCO3- exchanger	Heterochromatin formation, gene silencing (*BAHD1*)	Protein phosphatase regulatory subunit	Endothelial protein disulfide isomerase
Gene expression (www.gtexportal.org)	Ubiquitously expressed with highest expression in: pituitary, minor salivary gland, vagina, cervix, aorta, brain.	Brain (only)	*BAHD1* is ubiquitously expressed with highest expression in ovary, testis, thyroid, uterus, adrenal gland, fallopian tube. *RET* is expressed in brain, pituitary, colon and testis.	Ubiquitously expressed with highest expression in tibial arteries, brain, bladder, cervix, uterus, thyroid.	Ubiquitously expressed with lowest expression in brain.
WES	No	Yes	No	No	Yes
Physical parameters	small for gestational age (SGA), currently (2.4 years) weight <3rd centile; height 10th centile.	Normal	Low birth weight and disproportional length, currently normal.	Slightly underweight at birth; currently weight and height at 3rd–10th centiles.	None
ID/DD	Not observed	Moderate	Severe	Mild	Severe
Other neurological features	Hypotonia	Speech delay, hyperactivity, balance disorder, strange behaviour (sniffing)	Developmental regression, psychiatric disturbance, abnormal EEG, unspecific MRI changes	Personality disorder, self-mutilation	Lack of speech, lack of ambulation, seizures
Congenital anomalies	Bilateral cloudy cornea, supravalvular pulmonary stenosis, atrial septal defect, portosystemic venous shunt	Astigmatism	None	Retinal dystrophy, hyperopia, astigmatism	Microcephaly, corpus callosum hypoplasia
Dysmorphism	Square face, high forehead, bilateral epicanthic folds, sparse eyebrows, short and upturned nose, long and flat philtrum, narrow upper lip	Distal hand camptodactyly, unilateral transverse palmar crease	Large, soft and narrow hands with mild shortening of the metacarpals, long tapering fingers	Subtle hirsutism, low neck hairline, coarse face, rounded nasal tip, very broad thumbs (maternal feature), bilateral transverse palmar creases	None
Other	Not observed	Not observed	Urinary tract infection (UTI), septic ileus, Hirschsprung disease	aCGH: dup3p22pat, history of recurrent infections	None
References	23–31	1432–36	37–40	41–44	45–47

*pLI denotes the probability that a gene will be intolerant of loss-of-function mutations. The higher the pLI, the less tolerant the gene is of loss-of-function mutations.
#DOMINO score denotes the probability of a gene to harbor dominant mutations. The higher the score is, the more probable that the gene causes a disease with dominant inheritance.
aCGH, array comparative genomic hybridisation; DD, developmental delay; EEG, electroencephalography; ExAC, Exome Aggregation Consortium (http://exac.broadinstitute.org/); ID, intellectual delay; WES, whole-exome sequencing.

Table 2 Characteristics of the probands with breakpoints in genes with known impact on phenotype

	Proband 6	Proband 7	Proband 8	Proband 9
Current age	8 years	5 years	10 months	34 years
Karyotype	46, XY,t(10;22)(q26.1;q12.3)	46,XX,t(1;16)(p13.2;q13)	46,XY,t(5;8)(p13;q21.2)	46,XY,t(2;8)(q31;q24.1)
Implicated gene(s)	*EBF3, LARGE*	*ZNF423*	*NIPBL*	*TRPS1*
MIM number*	607407 (*EBF3*), 603590 (*LARGE*)	604557	608667	604386
WES	No	No	No	No
Physical parameters	Low birth weight, currently normal	Normal at birth, FTT, currently low weight and short for age	Prenatal growth retardation, low birth weight (1840 g). Recently failure to thrive, low weight, low-pitched, growling cry in infancy, sensorineural hearing loss.	Normal
ID/DD	Moderate	Moderate	Moderate	Not observed
Other neurological features	Neonatal hypotonia and later hypertonicity, speech delay, ADHD, fits of anger, abnormal EEG	Hypotonia, sound hypersensitivity, hyperactivity, speech delay, autistic features	Hypertonia in neonatal period, psychomotor developmental delay	None
Congenital anomalies	Total anomalous pulmonary venous return (TAPVR)	Hypoplastic thumbs, unilateral thumb symphalangism, strabismus and hyperopia, brain MRI (at 5 years): slightly dilated frontal horns and bodies of the lateral ventricles, small anterior pituitary lobe	Four hypoplastic fingers and a single transverse palmar crease on the left hand; bilateral cryptorchidism; atrial septal heart defect (ASD), gastro-oesophageal reflux, hirsutism	None
Dysmorphism	Tall forehead, straight eyebrows, narrow palpebral fissures, unilateral epicanthic fold. Anteverted short nostrils, thin lips with downturned corners of the mouth, short and broad chin, short hands, pes planovalgus, square toes with sandal gap.	Short palpebral fissures, telecanthus, flat and wide nose, hypoplastic nasal alae, low-set ears, micrognathia, high palate, hypertelorism.	Typical CdLS phenotype: microcephaly, synophrys, deep-set eyes, long eyelashes, long and prominent philtrum, microretrognathia	Typical frontal bulbous pear-shaped nose, broad philtrum, thin upper lip, large ears, hand and foot brachydactyly, broad thumbs and big toes, funnel chest
Diagnosis	*EBF3* delayed development syndrome (MIM: 617330)	Atypical disease from the *ZNF423* spectrum (MIM: 614844)?	Cornelia de Lange syndrome (MIM: 122470)	Trichorhinophalangeal syndrome (MIM: 190350)
Other	Urinary bladder malfunction, coprophilia	None	None	None

*Online Mendelian Inheritance in Man (OMIM, https://www.omim.org/).
ADHD, attention-deficit/hyperactivity disorder; DD, developmental delay; EEG, electroencephalography; FTT, failure to thrive; ID, intellectual delay; WES, whole-exome sequencing.

(50th centile), height 57 cm (>97th centile) and head circumference 32 cm (3rd centile). The pregnancy was uncomplicated apart from smaller OFC in fetal ultrasonography examinations. In neonatal period, microcephaly and hypotonia were observed which subsided after the first year. No congenital defects were noted after birth. Epileptic seizures refractory to treatment occurred from the 12th month. Brain MRI at 9 months showed hypoplasia of frontal part of corpus callosum. Control MRI at 7 years was normal. She has never achieved sitting, walking or speaking; sleep disturbances and excessive salivation were noted in infancy and throughout childhood. At the last follow-up, at 8 years, her weight was 16 kg (<3rd centile), length 138 cm (75th–90th centiles) and head circumference 48 cm (<3rd centile); she was without eye contact or verbal communication.

METHODS

Sample preparation

DNA of nine probands and their parents was isolated with the salting out method. Prior to SGMPS, karyotype analysis and aCGH were performed. aCGH was performed using commercially available arrays (CytoSure, Constitutional v3 (8×60 k), Oxford Gene Technology, Oxfordshire, UK, for all patients except probands 2 and 3 for whom Agilent Technologies SurePrint G3 CGH+SNP (4×180K) was used). CytoGenomics V.4.0.3.12 software was used for genomic copy-number analysis.

Mate pair library preparation and sequencing

Up to 1 µg of high-quality genomic DNA was used for library generation with the Mate Pair Library Preparation Kit (Illumina, San Diego, CA, USA) according to the manufacturer's instructions. The insert size length obtained varied from 2 to 4 kb. Mate-pair library was paired-end sequenced (2×100 bp) on Illumina HiSeq1500. Raw sequence reads were converted to the fastq format using the Illumina bcl2fastq program. After the quality control step, including adapter trimming and low-quality reads removal, reads were mapped to the reference genome (hg19) using bowtie2.[15] Each read from read pair was mapped independently and only unique mapped reads were used for further analysis. The .bam file was used for narrowing down the region where the translocations were located. A custom-made package for the programming language 'R' was applied for detection of discordant reads (paired reads where one read of the pair maps to one chromosome and the second read maps to another chromosome). Only clusters of 15 or more similar discordant reads between chromosomes with the translocation were further analysed. For visual verification of the results Integrative Genomics Viewer (IGV) was used.[16]

Whole-exome sequencing

In two probands whole-exome sequencing (WES) was performed, as SGMPS did not fully explain the phenotype of the patient. WES library was paired-end sequenced (2×100 bp) on Illumina HiSeq 1500, with the enrichment performed with SureSelect Human All Exon v5 kit (Agilent, Santa Clara, CA, USA) according to the manufacturer's instructions. Bioinformatic analysis was conducted as described previously.[17]

Validation of the SGMPS results

Validation of the results of SGMPS was performed using Sanger sequencing. The PCR primers were designed using Primer3Plus

(http://www.bioinformatics.nl/cgi-bin/primer3plus/primer3plus.cgi). Primer sequences and conditions for the PCR reaction are available on request. Verification of the specificity of the primers was performed using Primer Blast programme (https://www.ncbi.nlm.nih.gov/tools/primer-blast/). Samples for Sanger sequencing were prepared with BigDye Terminator v3.1 Cycle Sequencing Kit (Applied Biosystems, Foster City, USA) and analysed on 3500xL Genetic Analyzer (Applied Biosystems). Results were assessed with Variant Reporter V.1.1 software. Verification of the de novo status of the BCTs was confirmed using PCR reaction specific for the translocation. Parenthood was verified using AmpFLSTR NGM kit (Thermo Fisher Scientific) according to the manufacturer's instructions. The status of single nucleotide variants was verified by deep amplicon sequencing in both the parents and the probands. PCR amplification and design of the primers were done as described above. The library was prepared with Nextera XT (NXT) DNA Preparation Kit (Illumina), and paired-end sequenced (2×100 bp) on Illumina HiSeq1500. Analysis of NXT results was conducted manually with IGV. Detected translocations (figure 1) were called using a newly proposed genomic nomenclature for structural chromosomal rearrangements detected by NGS.[18] The likelihood that a gene was sensitive to mutation/deregulation of a single allele was estimated using pLI score from Exome Aggregation Consortium (ExAC)[19] and the recently proposed DOMINO score.[20]

Fibroblasts culture and RNA analysis

Skin fibroblasts from proband 3 were cultivated in cell culture flasks containing Dulbecco's Modified Eagle's Medium and Nutrient Mixture F-12, supplemented with 10% fetal bovine serum and penicillin/streptomycin 100 U/mL (GIBCO, BRL, Grand Island, NY, USA). The culture was sustained at 37°C/5% CO_2 until 80%–90% confluency. Isolation of the RNA from fibroblasts was conducted with TRIzol Reagent (Life Technologies, Carlsbad, California, USA) in accordance with the manufacturer's instructions. Reverse transcription was carried out with High-Capacity cDNA Reverse Transcription Kit (Life Technologies). The PCR reaction and Sanger sequencing of the amplified cDNA were performed as described in 'Validation of the SGMPS results'.

TAD analysis

TADs were detected with Insulation Score method[21] using Hi-C data from human GM12878 B-lymphoblastoid cells.[22] Plots showing genomic regions flanking the translocation breakpoints were generated by TADeus web service (http://bioputer.mimuw.edu.pl/tadeus, details in online supplementary methods).

Statistical analysis

In order to compare the distribution of pLI and DOMINO scores for genes which were directly disrupted in probands with potentially novel diseases (*EFNA5*, *BAHD1*, *PPP2R5E*, *TXNDC5*) versus all other human genes we performed a bootstrap test including 100 000 replicates on medians of the respective scores' values.

RESULTS

In all cases, BCT breakpoints were successfully mapped (online supplementary figure 1). Five out of nine analysed probands had breakpoint(s) in genes without a known disease phenotype. These patients are presented in detail below and in table 1. Additionally for these probands, TADs structure in the breakpoint region and characteristics of associated genes are presented in online supplementary file 1. The patients with breakpoints in genes with known disease associations which (in all cases) were consistent with clinically observed phenotype are presented in table 2.

Proband 1

SGMPS, based on 21 discordant reads and two split reads, defined the translocation as 46,XY,t(5;8)(q21.3:q11.21) with exact location for chromosome der(5): 46,XX,t(5;8)(q21.3:q11.21) dn.seq[GRCh37/hg19] t(5;8) (5pter→5q21.3 (106,748,346)::8q11.21 (55,326,842)→8qter); and for chromosome der(8): 46,XX,t(5;8) (q21.3:q11.21) dn.seq[GRCh37/hg19] t(5;8) (8pter→8q11.21 (55,326,759)::5q21.3 (106,748,356)→5qter). The breakpoint in chr5 is located in the third intron out of five introns of the *EFNA5* (MIM: 601535) gene, while the breakpoint in chr8 is located in non-coding DNA.

Proband 2

SGMPS, based on 20 discordant reads and one split read, defined the translocation as 46,XY,t(2;11)(q24.2;q21) with exact location for chromosome der(2): 46,XX,t(2;11)(q24.2:q21)dn.seq[GRCh37/hg19]t(2;11)(2pter→2q24.2 (162,667,703)::11q21(92,976,817)→11qter); and for chromosome der(11) 46,XX,t(2;11)(q24.2:q21)dn.seq[GRCh37/hg19]t(2;11)(11pter→11q21(92,976,811)::8q24.2 (162,667,701)→2qter). The breakpoint in chr2 is located in the fourth intron out of 26 introns of the *SLC4A10* (MIM: 605556) gene, while the breakpoint in chr11 is located in non-coding DNA. Based on the results from WES, four variants have been chosen for verification, but were excluded as disease candidates after family study (online supplementary table 1).

Proband 3

SGMPS, based on 15 discordant reads and one split read, defined the translocation as 46,XX,t(10;15)(q11.21;q15.1) with exact location for chromosome der(10): 46,XX,t(10;15)(q11.21:q15.1)dn.seq[GRCh37/hg19]t(10;15)(10pter→10q11.21 (43,594,152)::15q15.1 (40,735,863)→15qter); and for chromosome der(15) 46,XX,t(10;15)(q11.21:q15.1)dn.seq[GRCh37/hg19]t(10;15)(15pter→15q15.1 (40,735,866)::10q11.21(43,598,782)→10qter). The breakpoint in chr10 is located in the first intron out of 20 introns of the *RET* (MIM: 164761) gene, while the breakpoint in chr15 is in the second intron out of seven introns in the *BAHD1* (MIM: 613880) gene. In chromosome der(15), an insertion of around 500 bp, consisting of an intronic inverted fragment of *RET* gene, has been found. Sanger sequencing of the mRNA (cDNA) from fibroblasts identified expression of the fusion gene consisting of the promoter from *RET* gene and exons from *BAHD1* (figure 1D).

Proband 4

SGMPS, based on 27 discordant reads and one split read, defined the translocation as 46,XX,t(5,14)(q11.2;q23.2) with exact location for chromosome der(5): 46,XX,t(5,14)(q11.2;q23.2)dn.seq[GRCh37/hg19]t(5;14)(5pter→5q11.2 (54,203,477)::14q23.2 (63,908,907)→14qter); and for chromosome der(14) 46,XX,t(5,14)(q11.2;q23.2)dn.seq[GRCh37/hg19]t(5;14)(14pter→14q23.2 (63,908,904)::5q11.2 (54,203,482)→5qter). The breakpoint in chr5 is in non-coding DNA, while the breakpoint in chr14 is in the third intron out of 14 introns in the *PPP2R5E* (MIM: 601647) gene.

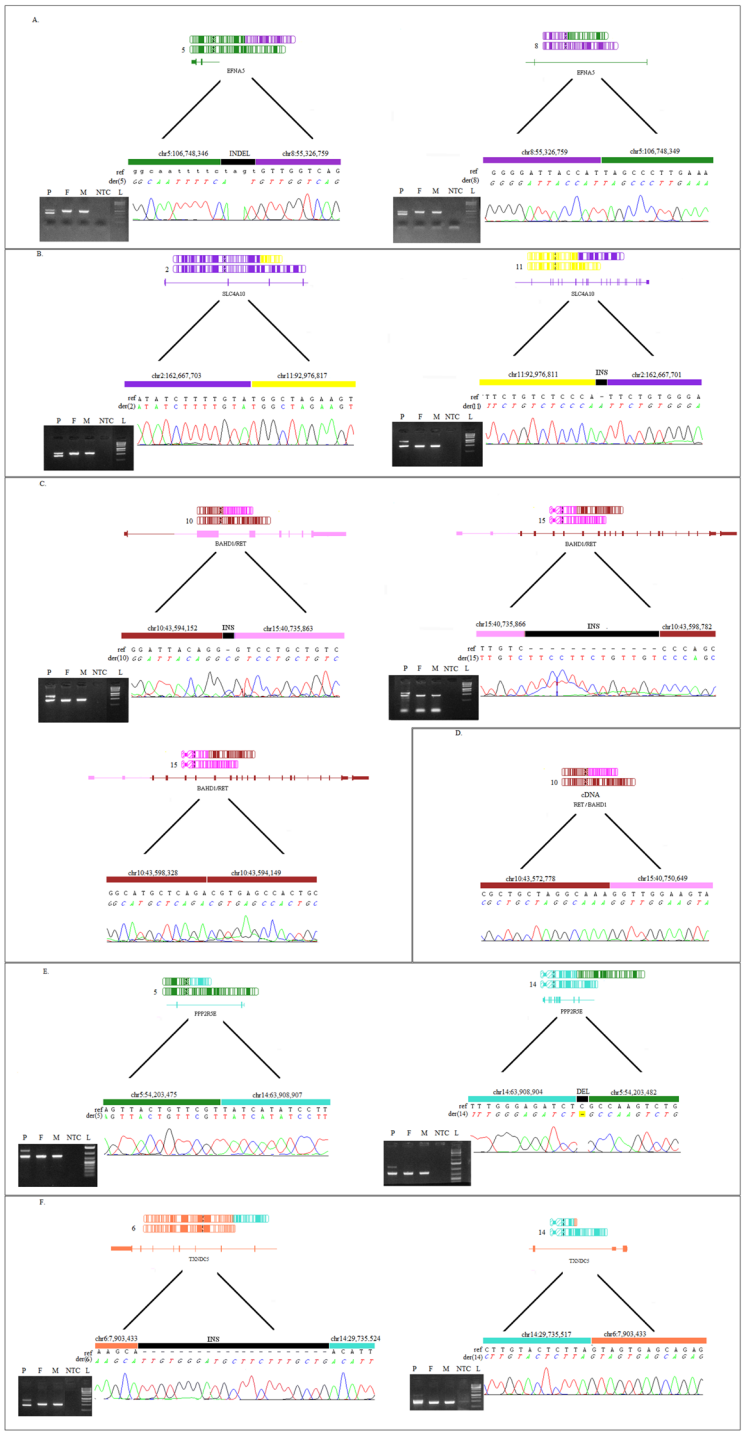

Figure 1 (A) Translocation between chromosomes 5 and 8 schematically shown with chromosome der5 on the right and der8 on the left. On the right of both der5 and der8 is Sanger sequencing validation of the breakpoint with the reference sequence. (B) Translocation between chromosomes 2 and 11 schematically shown with chromosome der2 on the right and der11 on the left. On the right of both der2 and der11 is Sanger sequencing validation of the breakpoint with the reference sequence. (C) Translocation between chromosomes 10 and 15 schematically shown with chromosome der10 on the right and der15 in the middle and on the left. On the right of both der10 and der15 is Sanger sequencing validation of the breakpoint with the reference sequence. The figure shows the 500 bp insertion at chromosome 10 with the structure of the breakpoint between the insertion and chromosome 10 and the breakpoint and chromosome 15. (D) cDNA product composed of *RET* promoter and the whole coding part of *BAHD1*. (E) Translocation between chromosomes 5 and 14 schematically shown with chromosome der5 on the left and der14 on the right. On the right of both der5 and der14 is Sanger sequencing validation of the breakpoint with the reference sequence. (F) Translocation between chromosomes 6 and 14 schematically shown with chromosome der6 on the left and der14 on the right. On the right of both der6 and der14 is Sanger sequencing validation of the breakpoint with the reference sequence. On the left of A, B, C and E are results of PCR screening using breakpoint specific primers. F, father; L, ladder; M, mother; NTC, non-template (negative) control; P, proband.

Proband 5

SGMPS, based on 17 discordant reads and two split reads, defined the translocation as 46,XX,t(6;14)(p25.1;q12) with exact location for chromosome der(6):

46,XX,t(6;14)(p25.1;q12)dn.seq[GRCh37/hg19]t(6;14)(14qter→14q12(29,735,524)::6p25.1 (7,903,434)→6qter); and for chromosome der(14) 46,XX,t(6;14)(p25.1;q12)dn.seq[GRCh37/hg19]t(6;14)(14pter→14q12(29,735,517)::6p25.1 (7,903,433)→2pter). The breakpoint in chr6 is located in the second intron out of nine introns of the *TXNDC5* (MIM: 616412) gene, while the breakpoint in chr14 is located in non-coding DNA. In der(6) an insertion of 19 bp is present at the breakpoint site (figure 1F). WES performed in the patient did not show the disease cause although we were not able to fully exclude the role of compound heterozygous mutations in *MTCL1* (online supplementary table 2).

The four genes which were directly disrupted in probands with potentially novel diseases (ie, *EFNA5, BAHD1, PPP2R5E, TXNDC5*) had significantly higher pLI ($p<0.017$) and DOMINO scores ($p<0.02$) than the remaining genes.

DISCUSSION

In all nine probands, 11 disrupted genes were found, that is, *EFNA5, EBF3* (MIM: 607407), *LARGE* (MIM: 603590), *PPP2R5E, TXNDC5, ZNF423* (MIM: 604557), *NIPBL* (MIM: 608667), *BAHD1, RET* (MIM:164761), *TRPS1* (MIM: 604386) and *SLC4A10* (see online supplementary table 3 for further characteristics of these genes). Five subjects had translocations that disrupted genes with unknown (*EFNA5, BAHD1, PPP2R5E, TXNDC5*) or poorly delineated impact on the phenotype (*SLC4A10*) and these are discussed below. The remaining translocations are discussed in the online supplementary discussion.

In proband 1 we suggest that the disease is caused by the truncation of *EFNA5*. EFNA5 (ephrin-5) belongs to a group of ephrin ligands that splits into two groups, EFNA and EFNB, depending on the structure and the way of membrane attachment.[23] *EFNA5* may be intolerant to monoallelic loss-of-function (LoF) mutations as suggested by pLI=0.89 (observed LoF variants −0, expected 7) and consistent with DOMINO score of 0.99. Ephrin receptors are important for the development of the central nervous system and growth of various types of blood vessels.[24 25] Seventeen per cent of homozygous *Efna5* knockout mice had dorsal midline defects in the form of perinatally lethal anencephaly or haematoma in the dorsal midline of the cranium.[26] The remaining knockout mice were apparently healthy but on close examination they harboured abnormalities of the lens and vitreous body of the eye.[26 27] The relevance of *EFNA5* for proper eye development is further underscored by reports that proper closure of the optic fissure[28] and retinal axon guidance[29] both require EFNA5 signalling.[30] Three rare (but not unique) *EFNA5* variants were associated with age-related cataracts in a study of 140 Chinese patients.[31] Thus, facial dysmorphy and vascular anomalies including persistent corneal fetal vascularisation and anomalies of heart and large vessels in our proband are broadly consistent with the known roles of ephrins/EFNA5 in encephalic/cranial pathology, vascular development and eye abnormalities.

In proband 2 the breakpoint in chromosome 2 was located in an intron of *SLC4A10*, while on chromosome 11 the breakpoint was found in non-coding DNA, thus suggesting that truncation of the *SLC4A10* gene caused the condition. Additionally, WES was performed in the proband because *SLC4A10* had features of a gene whose LoF should cause a recessive (PRec=0.997) rather than dominant disease (pLI=0.003, DOMINO=0.205). However, no mutations affecting the other copy of *SLC4A10* were found nor other variants which could explain the phenotype (online supplementary table 1). The *SLC4A10* gene belongs to the SLC4 transporter family and encodes an Na+ dependent transporter of Cl-HCO3- which likely affects the activity of neurons through a role in pH maintenance.[32] In mice *Slc4a10* knockout reduced brain ventricle volume and protected against fatal epileptic seizures.[32] Interestingly, in humans two cases of balanced translocations disrupting *SLC4A10* were described: t(2;13)(q24;q31) and t(1;2)(q42;q31).[14 33] In both cases, similar to our patient, developmental delay/mental retardation were found; in addition the first patient had epilepsy, while the second patient, in whom the *HHAT* (MIM: 605743) gene was additionally disrupted, had autism.[14 33] In both described patients, similar to our proband, there was no evidence for mutation affecting the second *SLC4A10* allele and the translocations breakpoint was located close to 5′ end of the gene (third, first and fourth introns, respectively). It is not clear why LoF of a single *SLC4A10* allele should be pathogenic when caused by a translocation but tolerated when caused by point mutations. One explanation could be related to the non-coding transcripts which originate from 5′ end of the *SLC4A10* gene (ENST00000606386, ENST00000482861, ENST00000605990) whose expression could be deregulated by translocation. Another possibility is that the translocation disrupts chromatin structure influencing expression of neighbouring genes such as *KCNH7* (MIM: 608169, pLI=0.98, DOMINO score=0.91) associated with bipolar spectrum disorder and schizophrenia[34 35] and/or *TBR1* (MIM: 604616, pLI=0.99, DOMINO score=0.999)—a gene located in the same TAD as the breakpoint and associated with intellectual disability and autism.[36 37] In summary, we report the third patient with a translocation damaging the 5′ end of *SLC4A10* providing additional evidence linking this *locus* with a dominant neurodevelopmental disease.

In proband 3 the breakpoints damaged *RET* and *BAHD1*, and formed a fusion gene including the 5′ part of *RET* and 3′ part of *BAHD1*. Monoallelic *RET* mutations cause Hirschsprung disease (present in our proband) and hereditary cancer syndromes which may manifest in our proband later in life. As *RET* defects have not been linked with neurodevelopmental/psychiatric phenotypes, it is likely that these are caused by defect of *BAHD1*. BAHD1 is involved in epigenetic regulation through heterochromatin formation in interaction with HP1, MBD1 and HDAC5.[38 39] Expression of *BAHD1* is uniform in all tissues but is lowest in fetal brain.[40] In our patient, the 5′UTR from the *BAHD1* gene is fused with the 19 exons of *RET*, while the whole coding part of *BAHD1* is fused with the proximal part of *RET*. We found the *RET/BAHD1* fusion gene is expressed whereas we could not find the *BAHD1/RET* fusion product. Thus, in our proband *BAHD1* may be overexpressed enhancing heterochromatin formation which may be pathogenic.[39] Given the suggested role of *BAHD1* in immune system[41] it is also possible that recurrent infections in our proband are also part of the translocation phenotype.

In proband 4 we found a disruption of *PPP2R5E* encoding a regulatory subunit of the protein phosphatase 2A expressed in the brain and heart.[42–44] PPP2R5E might play a role in development of Alzheimer's disease (MIM: 104300)[42] and its depletion leads to destabilisation of MTCL1, a protein responsible for the regulation of microtubule organisation, which may be pathogenic.[45] No LoF variants of *PPP2R5E* were found in ExAC (expected number −21); both pLI score (0.9994) and DOMINO score (0.86) suggest that damage of a single copy of *PPP2R5E* may be pathogenic.

In proband 5 the breakpoint was located in a conjoined gene *BLOC1S5-TXNDC5* and was predicted to damage both the shRNA transcript and the *TXNDC5* gene. Despite biologically important role of *TXNDC5* for disulphide bond formation in proteins[46] the gene is not expected to cause a dominant disease (pLI=0, DOMINO=0.14). WES, together with family studies, showed the disease in proband 5 could potentially be caused by biallelic *MTCL1* gene variants (MIM: 615766, online supplementary table 2). *MTCL1* is involved in axon formation,[47] however it has not been linked to human disease and the detected variants are predicted to be benign. Considering this, we speculate that the disease in proband 5 could be caused by LRPE. Interestingly, the TAD disrupted by the breakpoint in chr14 contains *FOXG1* (MIM: 164874) whose monoallelic defects (including LoF variants) cause neurodevelopmental disorders with mental retardation, epilepsy and/or congenital Rett-like symptoms (MIM: 613454, online supplementary file 1).[48]

The finding that the four genes which were directly disrupted in probands with potentially novel diseases (ie, *EFNA5*, *BAHD1*, *PPP2R5E*, *TXNDC5*) had significantly higher pLI and DOMINO scores than the remaining genes indicates an enrichment in genes most likely to cause diseases with autosomal dominant inheritance. This, independently from other considerations, suggests that the defects of at least some of these genes do contribute to observed disease phenotypes.

In conclusion, we confirm the usefulness of SGMPS for analysis of BCTs and detection of novel candidate genes for dominant human disorders.

Electronic database information

- OMIM: https://www.omim.org.
- ExAC: http://exac.broadinstitute.org.
- VarSome: https://varsome.com/.
- GTExPORTAL: www.gtexportal.org.

Author affiliations
[1]Department of Medical Genetics, Medical University of Warsaw, Warsaw, Poland
[2]Postgraduate School of Molecular Medicine, Medical University of Warsaw, Warsaw, Poland
[3]Department of Medical Genetics, The Children's Memorial Health Institute, Warsaw, Poland
[4]Faculty of Mathematics, Informatics and Mechanics, Institute of Informatics, University of Warsaw, Warsaw, Poland
[5]Department of Pediatrics, Medical University of Warsaw, Warsaw, Poland
[6]genXone, Poznan, Poland
[7]Department of Clinical Genetics, Podlaskie Medical Center, Bialystok, Poland
[8]Department of Perinatology, Medical University of Bialystok, Bialystok, Poland
[9]Department of Forensic Medicine, Medical University of Warsaw, Warsaw, Poland
[10]Department of Medical Genetics, Institute of Mother and Child, Warsaw, Poland
[11]Department of Diagnostic Imaging, The Children's Memorial Health Institute, Warsaw, Poland
[12]Department of Pediatrics and Rare Disorder, Wroclaw Medical University, Wroclaw, Poland

Acknowledgements The authors are grateful to the patients and the parents for allowing this study to be published.

Contributors VMP, KS, RPo, RPl, MKW, RS, AG, JC, BP and AS wrote the manuscript. VMP, MK and MM performed the experiments. RPl, MR, AG, KC and MKW designed the experiment. VMP, MK and MM designed the pipeline. VMP, BP, AG and MS performed bioinformatic analysis. MM, MK, AS, RPo, PK, JC, EW, RS, KC and MKW contacted the patients. VMP, MR, AAK, AB, AW and JK performed next-generation sequencing. EJ preformed MRI analysis.

Funding The research was supported by the National Science Centre (NCN) grant number 2016/21/B/NZ5/02541.

Competing interests None declared.

Patient consent Parental/guardian consent obtained.

Ethics approval Ethics approval for the study was granted by the Ethical Committee at the Medical University of Warsaw (KB/127/2017).

Provenance and peer review Not commissioned; externally peer reviewed.

REFERENCES

1. Staff PO. PLOS ONE Staff. Correction: Accurate Breakpoint Mapping in Apparently Balanced Translocation Families with Discordant Phenotypes Using Whole Genome Mate-Pair Sequencing. *PLoS One* 2017;12:e0174190.
2. Warburton D. De novo balanced chromosome rearrangements and extra marker chromosomes identified at prenatal diagnosis: clinical significance and distribution of breakpoints. *Am J Hum Genet* 1991;49:995–1013.
3. Halgren C, Nielsen NM, Nazaryan-Petersen L, Silahtaroglu A, Collins RL, Lowther C, Kjaergaard S, Frisch M, Kirchhoff M, Brøndum-Nielsen K, Lind-Thomsen A, Mang Y, El-Schich Z, Boring CA, Mehrjouy MM, Jensen PKA, Fagerberg C, Krogh LN, Hansen J, Bryndorf T, Hansen C, Talkowski ME, Bak M, Tommerup N, Bache I. Risks and Recommendations in Prenatally Detected De Novo Balanced Chromosomal Rearrangements from Assessment of Long-Term Outcomes. *Am J Hum Genet* 2018;102:1090–103.
4. Harewood L, Chaignat E, Reymond A. Structural variation and its effect on expression. *Methods Mol Biol* 2012;838:173–86.
5. Mitelman F, Johansson B, Mertens F. The impact of translocations and gene fusions on cancer causation. *Nat Rev Cancer* 2007;7:233–45.
6. Mertens F, Johansson B, Fioretos T, Mitelman F. The emerging complexity of gene fusions in cancer. *Nat Rev Cancer* 2015;15:371–81.
7. Nothwang HG, Kim HG, Aoki J, Geisterfer M, Kübart S, Wegner RD, van Moers A, Ashworth LK, Haaf T, Bell J, Arai H, Tommerup N, Ropers HH, Wirth J. Functional hemizygosity of PAFAH1B3 due to a PAFAH1B3-CLK2 fusion gene in a female with mental retardation, ataxia and atrophy of the brain. *Hum Mol Genet* 2001;10:797–806.
8. Eykelenboom JE, Briggs GJ, Bradshaw NJ, Soares DC, Ogawa F, Christie S, Malavasi EL, Makedonopoulou P, Mackie S, Malloy MP, Wear MA, Blackburn EA, Bramham J, McIntosh AM, Blackwood DH, Muir WJ, Porteous DJ, Millar JK. A t(1;11) translocation linked to schizophrenia and affective disorders gives rise to aberrant chimeric DISC1 transcripts that encode structurally altered, deleterious mitochondrial proteins. *Hum Mol Genet* 2012;21:3374–86.
9. Lettice LA, Daniels S, Sweeney E, Venkataraman S, Devenney PS, Gautier P, Morrison H, Fantes J, Hill RE, FitzPatrick DR. Enhancer-adoption as a mechanism of human developmental disease. *Hum Mutat* 2011;32:1492–9.
10. Harewood L, Schütz F, Boyle S, Perry P, Delorenzi M, Bickmore WA, Reymond A. The effect of translocation-induced nuclear reorganization on gene expression. *Genome Res* 2010;20:554–64.
11. Harewood L, Fraser P. The impact of chromosomal rearrangements on regulation of gene expression. *Hum Mol Genet* 2014;23(R1):R76–R82.
12. Martin CL, Warburton D. Detection of Chromosomal Aberrations in Clinical Practice: From Karyotype to Genome Sequence. *Annu Rev Genomics Hum Genet* 2015;16:309–26.
13. Le Scouarnec S, Gribble SM. Characterising chromosome rearrangements: recent technical advances in molecular cytogenetics. *Heredity* 2012;108:75–85.
14. Nilsson D, Pettersson M, Gustavsson P, Förster A, Hofmeister W, Wincent J, Zachariadis V, Anderlid BM, Nordgren A, Mäkitie O, Wirta V, Käller M, Vezzi F, Lupski JR, Nordenskjöld M, Lundberg ES, Carvalho CMB, Lindstrand A. Whole-Genome Sequencing of Cytogenetically Balanced Chromosome Translocations Identifies Potentially Pathological Gene Disruptions and Highlights the Importance of Microhomology in the Mechanism of Formation. *Hum Mutat* 2017;38:180–92.
15. Langmead B, Salzberg SL. Fast gapped-read alignment with Bowtie 2. *Nat Methods* 2012;9:357–9.
16. Thorvaldsdottir H, Robinson JT, Mesirov JP, Viewer IG. IGV): high-performance genomics data visualization and exploration. *Brief Bioinform* 2013;14:178–92.
17. Ploski R, Pollak A, Muller S, Franaszczyk M, Michalak E, Kosinska J, Stawinski P, Spiewak M, Seggewiss H, Bilinska ZT. Does p. *Q247X in TRIM63 cause human hypertrophic cardiomyopathy? Circ Res* 2014;114:e2–5.
18. Ordulu Z, Wong KE, Currall BB, Ivanov AR, Pereira S, Althari S, Gusella JF, Talkowski ME, Morton CC. Describing sequencing results of structural chromosome rearrangements with a suggested next-generation cytogenetic nomenclature. *Am J Hum Genet* 2014;94:695–709.
19. Lek M, Karczewski KJ, Minikel EV, Samocha KE, Banks E, Fennell T, O'Donnell-Luria AH, Ware JS, Hill AJ, Cummings BB, Tukiainen T, Birnbaum DP, Kosmicki JA, Duncan LE, Estrada K, Zhao F, Zou J, Pierce-Hoffman E, Berghout J, Cooper DN, Deflaux N, DePristo M, Do R, Flannick J, Fromer M, Gauthier L, Goldstein J, Gupta N, Howrigan D, Kiezun A, Kurki MI, Moonshine AL, Natarajan P, Orozco L, Peloso GM, Poplin R, Rivas MA, Ruano-Rubio V, Rose SA, Ruderfer DM, Shakir K, Stenson PD, Stevens C, Thomas BP, Tiao G, Tusie-Luna MT, Weisburd B, Won HH, Yu D, Altshuler DM, Ardissino D, Boehnke M, Danesh J, Donnelly S, Elosua R, Florez JC, Gabriel SB, Getz G, Glatt SJ, Hultman CM, Kathiresan S, Laakso M, McCarroll S, McCarthy MI, McGovern D, McPherson R, Neale BM, Palotie A, Purcell SM, Saleheen D, Scharf JM, Sklar P, Sullivan PF, Tuomilehto J, Tsuang MT, Watkins HC, Wilson JG, Daly MJ, MacArthur DG. Exome

Aggregation Consortium. Analysis of protein-coding genetic variation in 60,706 humans. *Nature* 2016;536:285–91.
20. Quinodoz M, Royer-Bertrand B, Cisarova K, Di Gioia SA, Superti-Furga A, Rivolta C. DOMINO: Using Machine Learning to Predict Genes Associated with Dominant Disorders. *Am J Hum Genet* 2017;101:623–9.
21. Crane E, Bian Q, McCord RP, Lajoie BR, Wheeler BS, Ralston EJ, Uzawa S, Dekker J, Meyer BJ. Condensin-driven remodelling of X chromosome topology during dosage compensation. *Nature* 2015;523:240–4.
22. Rao SS, Huntley MH, Durand NC, Stamenova EK, Bochkov ID, Robinson JT, Sanborn AL, Machol I, Omer AD, Lander ES, Aiden EL. A 3D map of the human genome at kilobase resolution reveals principles of chromatin looping. *Cell* 2014;159:1665–80.
23. Cheng C, Gong X. Diverse roles of Eph/ephrin signaling in the mouse lens. *PLoS One* 2011;6:e28147.
24. Pasquale EB. Eph receptor signalling casts a wide net on cell behaviour. *Nat Rev Mol Cell Biol* 2005;6:462–75.
25. Kuijper S, Turner CJ, Adams RH. Regulation of angiogenesis by Eph-ephrin interactions. *Trends Cardiovasc Med* 2007;17:145–51.
26. Cooper MA, Son AI, Komlos D, Sun Y, Kleiman NJ, Zhou R. Loss of ephrin-A5 function disrupts lens fiber cell packing and leads to cataract. *Proc Natl Acad Sci U S A* 2008;105:16620–5.
27. Son AI, Sheleg M, Cooper MA, Sun Y, Kleiman NJ, Zhou R. Formation of persistent hyperplastic primary vitreous in ephrin-A5-/- mice. *Invest Ophthalmol Vis Sci* 2014;55:1594–606.
28. Noh H, Lee H, Park E, Park S. Proper closure of the optic fissure requires ephrin A5-EphB2-JNK signaling. *Development* 2016;143:461–72.
29. Frisén J, Yates PA, McLaughlin T, Friedman GC, O'Leary DD, Barbacid M. Ephrin-A5 (AL-1/RAGS) is essential for proper retinal axon guidance and topographic mapping in the mammalian visual system. *Neuron* 1998;20:235–43.
30. Hara Y, Nomura T, Yoshizaki K, Frisén J, Osumi N. Impaired hippocampal neurogenesis and vascular formation in ephrin-A5-deficient mice. *Stem Cells* 2010;28:974–83.
31. Lin Q, Zhou N, Zhang N, Qi Y. Mutational screening of EFNA5 in Chinese age-related cataract patients. *Ophthalmic Res* 2014;52:124–9.
32. Jacobs S, Ruusuvuori E, Sipilä ST, Haapanen A, Damkier HH, Kurth I, Hentschke M, Schweizer M, Rudhard Y, Laatikainen LM, Tyynelä J, Praetorius J, Voipio J, Hübner CA. Mice with targeted Slc4a10 gene disruption have small brain ventricles and show reduced neuronal excitability. *Proc Natl Acad Sci U S A* 2008;105:311–6.
33. Gurnett CA, Veile R, Zempel J, Blackburn L, Lovett M, Bowcock A. Disruption of sodium bicarbonate transporter SLC4A10 in a patient with complex partial epilepsy and mental retardation. *Arch Neurol* 2008;65:550–3.
34. Genovese G, Fromer M, Stahl EA, Ruderfer DM, Chambert K, Landén M, Moran JL, Purcell SM, Sklar P, Sullivan PF, Hultman CM, McCarroll SA. Increased burden of ultra-rare protein-altering variants among 4,877 individuals with schizophrenia. *Nat Neurosci* 2016;19:1433–41.
35. Strauss KA, Markx S, Georgi B, Paul SM, Jinks RN, Hoshi T, McDonald A, First MB, Liu W, Benkert AR, Heaps AD, Tian Y, Chakravarti A, Bucan M, Puffenberger EG. A population-based study of KCNH7 p.Arg394His and bipolar spectrum disorder. *Hum Mol Genet* 2014;23:6395–406.
36. McDermott JH, Study DDD, Clayton-Smith J, Briggs TA. The TBR1-related autistic-spectrum-disorder phenotype and its clinical spectrum. *Eur J Med Genet* 2018;61:253–6.
37. Hamdan FF, Srour M, Capo-Chichi JM, Daoud H, Nassif C, Patry L, Massicotte C, Ambalavanan A, Spiegelman D, Diallo O, Henrion E, Dionne-Laporte A, Fougerat A, Pshezhetsky AV, Venkateswaran S, Rouleau GA, Michaud JL. De novo mutations in moderate or severe intellectual disability. *PLoS Genet* 2014;10:e1004772.
38. Zhao D, Zhang X, Guan H, Xiong X, Shi X, Deng H, Li H. The BAH domain of BAHD1 is a histone H3K27me3 reader. *Protein Cell* 2016;7:222–6.
39. Bierne H, Tham TN, Batsche E, Dumay A, Leguillou M, Kernéis-Golsteyn S, Regnault B, Seeler JS, Muchardt C, Feunteun J, Cossart P. Human BAHD1 promotes heterochromatic gene silencing. *Proc Natl Acad Sci U S A* 2009;106:13826–31.
40. Nagase T, Ishikawa K, Suyama M, Kikuno R, Hirosawa M, Miyajima N, Tanaka A, Kotani H, Nomura N, Ohara O. Prediction of the coding sequences of unidentified human genes. XIII. The complete sequences of 100 new cDNA clones from brain which code for large proteins in vitro. *DNA Res* 1999;6:63–70.
41. Lebreton A, Lakisic G, Job V, Fritsch L, Tham TN, Camejo A, Matteï PJ, Regnault B, Nahori MA, Cabanes D, Gautreau A, Ait-Si-Ali S, Dessen A, Cossart P, Bierne H. A bacterial protein targets the BAHD1 chromatin complex to stimulate type III interferon response. *Science* 2011;331:1319–21.
42. Nematullah M, Hoda MN, Khan F. Protein Phosphatase 2A: a Double-Faced Phosphatase of Cellular System and Its Role in Neurodegenerative Disorders. *Mol Neurobiol* 2018;55.
43. Eichhorn PJ, Creyghton MP, Bernards R. Protein phosphatase 2A regulatory subunits and cancer. *Biochim Biophys Acta* 2009;1795:1–15.
44. Benoist M, Gaillard S, Castets F. The striatin family: a new signaling platform in dendritic spines. *J Physiol Paris* 2006;99(2-3):146–53.
45. Hyodo T, Ito S, Asano-Inami E, Chen D, Senga T. A regulatory subunit of protein phosphatase 2A, PPP2R5E, regulates the abundance of microtubule crosslinking factor 1. *Febs J* 2016;283:3662–71.
46. Horna-Terrón E, Pradilla-Dieste A, Sánchez-de-Diego C, Osada J. TXNDC5, a newly discovered disulfide isomerase with a key role in cell physiology and pathology. *Int J Mol Sci* 2014;15:23501–18.
47. Satake T, Yamashita K, Hayashi K, Miyatake S, Tamura-Nakano M, Doi H, Furuta Y, Shioi G, Miura E, Takeo YH, Yoshida K, Yahikozawa H, Matsumoto N, Yuzaki M, Suzuki A. MTCL1 plays an essential role in maintaining Purkinje neuron axon initial segment. *Embo J* 2017;36:1227–42.
48. Ariani F, Hayek G, Rondinella D, Artuso R, Mencarelli MA, Spanhol-Rosseto A, Pollazzon M, Buoni S, Spiga O, Ricciardi S, Meloni I, Longo I, Mari F, Broccoli V, Zappella M, Renieri A. FOXG1 is responsible for the congenital variant of Rett syndrome. *Am J Hum Genet* 2008;83:89–93.